Polymer 220 (2021) 123574

Contents lists available at ScienceDirect

Polymer

journal homepage: http://www.elsevier.com/locate/polymer

An effective nucleating agent for isotactic polypropylene (iPP): Zinc bis-(nadic anhydride) double-decker silsesquioxanes

Xian Zhang [a], Shicheng Zhao [a], Shiao-Wei Kuo [b], Wei-Cheng Chen [b], Mohamed Gamal Mohamed [b,c], Zhong Xin [a,*]

[a] Shanghai Key Laboratory of Multiphase Materials Chemical Engineering, Department of Product Engineering, East China University of Science and Technology, Shanghai 200237, People's Republic of China
[b] Department of Materials and Optoelectronic Science, National Sun Yat-Sen University, Kaohsiung 804, Taiwan
[c] Chemistry Department, Faculty of Science, Assiut University, Assiut 71516, Egypt

ARTICLE INFO

Keywords:
Isotactic polypropylene
POSS-based nucleating agent
Fast scanning calorimetry (FSC)

ABSTRACT

The zinc bicyclo [2.2.1]-heptane-2, 3-dicarboxylate-double-decker silsesquioxanes (Zn_2(DDSQ-ND)) was firstly synthesized and the crystallization behavior of isotactic polypropylene (iPP) filled with different amount of Zn_2(DDSQ-ND) (0–1 wt %) was investigated in detail. With the addition of Zn_2(DDSQ-ND), the crystallization temperature enhanced significantly, indicating that it acted novel and effective nucleating agent in the iPP system. The morphology of spherulites, nucleation density, and the crystal structure of the samples were characterized using POM and WAXD. Besides, ultra-fast scanning calorimetry (FSC) was employed to study the effects of Zn_2(DDSQ-ND) on the non-isothermal and isothermal crystallization behaviors of the sample iPP/Zn_2(DDSQ-ND) under the high cooling rates and wide crystallization temperature ranges, as well as the cold crystallization and recrystallization behavior during the heating process. The data suggested that Zn_2(DDSQ-ND) accelerated the formation of α-phase iPP and acted as a novel α-nucleating agent in the iPP system.

1. Introduction

Isotactic polypropylene (iPP) is an important commercial resin and has been widely used in many scopes such as packaging, machinery, transportation, electrical field due to its excellent performance [1]. To further expand its application, the method of physical blending or copolymerization is usually conducted to modify iPP. As a typical semi-crystalline polymer, the properties of iPP largely depend on crystallization behavior [2–5]. The addition of a nucleating agent (NA) through physical blending is one of the most popular and cost-efficient ways to accelerate the crystallization process and modify the properties of iPP. NA can increase the crystallization temperature and reduce the crystals size of the polymer, which leads to a general improvement of processability and mechanical properties of the final product [6–10]. Nowadays, the development of high-efficiency NA for semi-polymer is still an attractive research direction in industry and academia.

Polyhedral oligomeric silsesquioxanes (POSS) are organic-inorganic hybrid nano-particles, which have attracted great attention in recent years as novel nanofillers [11]. It has the empirical formula of $(RSiO_{1.5})_n$ where R is an active or inert organic group covalently attached to inorganic Si–O core [12,13]. Due to the great flexibility of its structures, POSS has attracted much attention in the field of polymer modification [14–16]. The introduction of POSS can greatly improve the properties of the polymer, such as mechanical properties, thermal stability, thermo-oxidative resistance, decreased flammability, and viscosity [17,18]. The different cage structures and functional groups around the core result in a wide variety of POSS. So far, there are more than one hundred kinds of commercialized POSS. Besides, it is reported that POSS can act as a nucleating agent for semi-crystalline polymers and accelerate the crystallization process [11,19–22]. It is well-known that the functional groups of POSS significantly affect its nucleation efficiency in polymer matrixes [21,23,24]. In the literature, the molecular structure containing metal carboxylate is frequently reported as an effectively nucleating agent for iPP, such as zinc phthalate [25], zinc adipate [26], Al-PTBBA [27], and carboxylated graphene/calcium pimelate [28]. However, the potential of POSS with bicyclo [2.2.1]-heptane-2,3-dicarboxylate functional group as an effective nucleating agent has not been explored. In our study, it was first synthesized and its effect on the crystallization

* Corresponding author.
E-mail address: xzh@ecust.edu.cn (Z. Xin).

https://doi.org/10.1016/j.polymer.2021.123574
Received 24 November 2020; Received in revised form 22 February 2021; Accepted 25 February 2021
Available online 28 February 2021
0032-3861/

behavior with iPP was focused analyzed here.

Besides, the nucleating efficiency of NA largely depends on the cooling rate and the temperature of crystallization [29,30]. The ultra-fast scanning calorimetry (FSC) can provide us a better understanding of the crystallization behavior of iPP with the POSS-based NA under a high cooling rate or a wide crystallization temperature range.

In this section, we synthesized zinc bicyclo [2.2.1]-heptane-2, 3-dicarboxylate-double-decker silsesquioxanes (Zn_2(DDSQ-ND)) firstly and prepared iPP/Zn_2(DDSQ-ND) hybrid materials by melt blending. The crystallization behavior of Zn_2(DDSQ-ND) in the iPP system was enlarged investigated by combining differential scanning calorimetry (DSC) and FSC. The morphologies and crystal structure of iPP samples were analyzed using polarized optical microscopy (POM) and wide-angle X-ray scattering (WAXD), respectively. In addition, the influence of Zn_2(DDSQ-ND) on the non-isothermal and isothermal crystallization behaviors of iPP was also measured using FSC under a high cooling rate and a wide crystallization temperature range.

2. Experimental

2.1. Materials

In this study, the commercial iPP (trade name T30S, $M_w = 4.51 \times 10^5$ g mol^{-1}, PDI = 3.51) was supplied by Jiujiang Petroleum Chemical (China) with a melt flow index (MFI) of 2.9 g/10 min (230 °C/2.16 kg). The syntheses of bis-(nadic anhydride) double-decker silsesquioxanes (DDSQ-ND) are described in Ref. [31]. Zinc oxide (ZnO) was obtained from Shanghai Titanchem Co., Ltd. (China). Tetrahydrofuran was obtained from Shanghai Titan Science Corp. All chemicals were of analytical grade and used without further purification.

2.2. Synthesis of zinc bicyclol [2.2.1]-heptane-2, 3-dicarboxylate-double-decker silsesquioxanes (Zn_2(DDSQ-ND))

As shown in Scheme 1, Zinc salt of bis-(nadic anhydride) double-decker silsesquioxanes (Zn_2(DDSQ-ND)) was synthesized according to the similar reaction [25]. Bis-(nadic anhydride) double-decker silsesquioxanes (DDSQ-ND) (1.0 g, 0.6 mmol) and zinc oxide (ZnO) (0.1 g, 1.2 mmol) were dissolved in tetrahydrofuran (50 mL) and stirred at 70 °C for 8 h. Then the solvent was removed using vacuum distillation. After that, white powder was obtained after washing using fresh tetrahydrofuran. The obtained product was dried at 70 °C under a vacuum oven for 24 h (yield: 80.6%). The structure, thermostability, and crystal morphology of Zn_2(DDSQ-ND) were characterized by Fourier transform infrared spectroscopy (FT-IR), wide-angle X-ray diffraction (WAXD), thermogravimetric analysis (TGA), and scanning electron microscopy (SEM), as shown in Fig. 1, S1-3. The results indicated that Zn_2(DDSQ-ND) with the single crystal plate and multi-layer assembled block crystal morphology were synthesized and exhibited high thermal stability at the processing condition. Based on the results of WAXD, the crystal form of Zn_2(DDSQ-ND) obviously changed compared with DDSQ-ND, which also confirmed DDSQ-ND reacted with ZnO. The FT-IR spectra were recorded on a Nicolet iS10 FT-IR spectrometer (the United States) using KBr pellets in the range of 4000−500 cm^{-1}. IR data (ν/cm^{-1}): 1644, 1622 [ν(COO−)$_{as}$], 1449 [ν(COO−)$_s$], 1266, 1131, 1027.

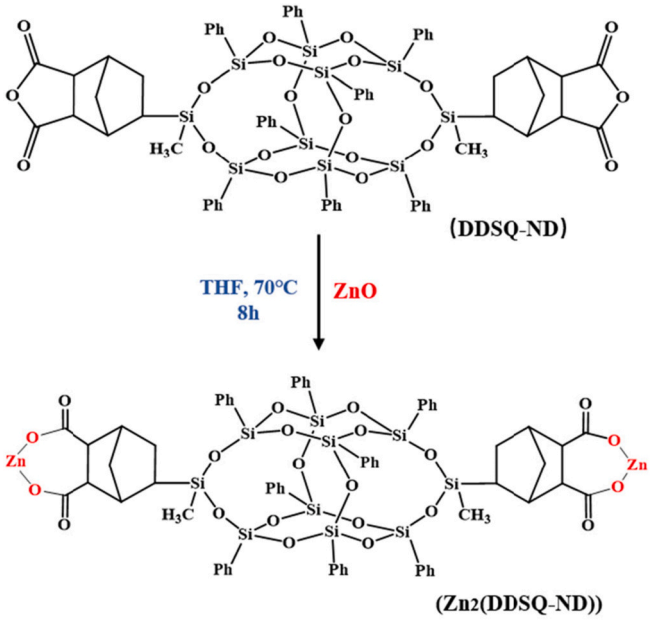

Scheme 1. Synthetic route of Zn_2(DDSQ-ND).

2.3. Preparation of iPP/Zn_2(DDSQ-ND) composites

The iPP was mixed with 0, 0.05, 0.1, 0.2, 0.4, 0.6, 0.8 and 1 wt % nucleating agent Zn_2(DDSQ-ND), respectively. The powdery PP and Zn_2(DDSQ-ND) was pre-mixed fully using the method of dry-blended. Then, the compound further mixed using a twin-screw extruder (Haake Minilab, Thermal Fisher Scientific (China) Co., Ltd.) at 200 °C and a rotating speed of 60 rpm.

2.4. Characterizations

The crystallization and melting behaviors of samples were investigated using a differential scanning calorimeter (DSC3+, METTLER TOLEDO, Switzerland) under the protection of nitrogen flow (150 mL min^{-1}). The temperature was calibrated using indium (In) as a standard medium before measurements. The samples (3–5 mg) were heated to 200 °C and kept at this temperature for 5 min to eliminate the thermal history. Then the samples were cooled to 50 °C at a cooling rate of 10 °C·min^{-1} and reheated to 200 °C at a heating rate of 10 °C·min^{-1}. The heat flow as a function of temperature was recorded. Besides, ultra-fast scanning calorimetry (FSC) experiments were performed using a Mettler Toledo Flash DSC 1 apparatus fitted with a UFS 1 sensor. Figs. 2 and 3 displayed the temperature-time profile for non-isothermal and isothermal crystallization experiments. All operations were conducted under the protection of the nitrogen atmosphere. The samples were

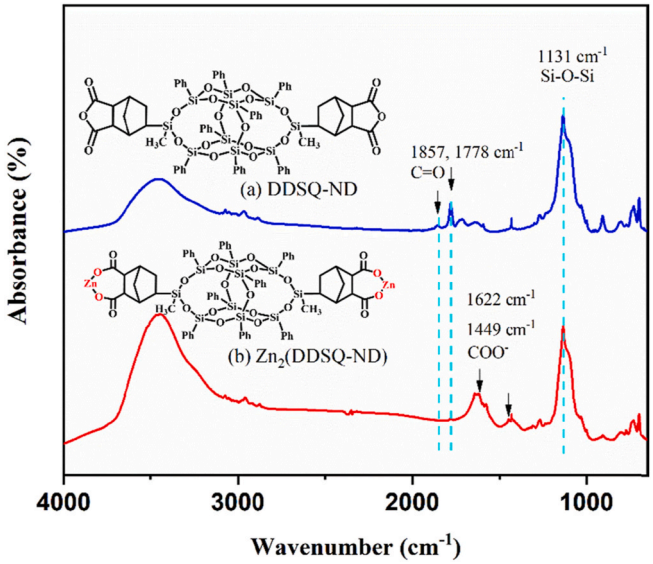

Fig. 1. FTIR spectra of DDSQ-ND and Zn_2(DDSQ-ND).

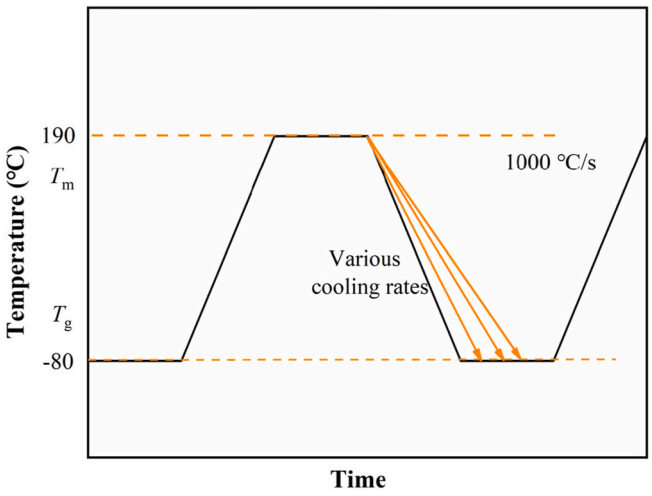

Fig. 2. Temperature-time profile for non-isothermal crystallization of iPP at different cooling rates.

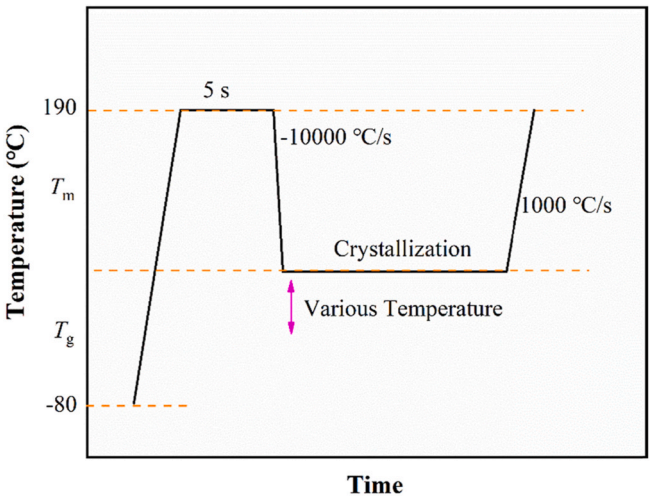

Fig. 3. Temperature-time profile for isothermal crystallization of iPP under various temperature.

prepared under a microscope and support temperature was set to −90 °C. The typical sample size was between 20 and 200 ng [32]. Wide-angle X-ray diffraction (WAXD) was carried out using a Rigaku D/max-2550VB/PC apparatus (Japan). The spectra were recorded in the 2θ range of 5–50° by using Cu Kα radiation (λ = 1.54 Å). Morphologies of iPP samples were obtained using a polarized optical microscope (BX51 Olympus) equipped with a digital camera (DP70). A Linkam (THMS600) hot stage was used to control the experimental temperature. The samples were kept at 200 °C for 5 min to erase the thermal history. Then, the samples were cooled to 141 °C at the maximum cooling rate of the machine and maintained at 141 °C until the crystallization was completed.

3. Results and discussion

3.1. Nucleation efficiency of the Zn_2(DDSQ-ND)

The crystallization processes of isotactic polypropylene (iPP) with zinc bicyclo [2.2.1]-heptane-2, 3-dicarboxylate-double-decker silsesquioxanes (Zn_2(DDSQ-ND)) (0–1 wt %) were investigated using conventional differential scanning calorimetry (DSC). Fig. 4 displays the crystallization and melting behavior of iPP with different content of Zn_2(DDSQ-ND). The presents of Zn_2(DDSQ-ND) increases the temperature of the crystallization peak (T_c). Generally, the T_c of the polymer is one of the vital criteria to determine the nucleating efficiency of the nucleating agent (NA). As reported, if the T_c value of the polymer containing 1% of additive is 6.5 °C or more higher than that of the polymer alone, the nucleating efficiency of the additives is rated as high [33]. Fig. 5 presents the dependence of T_p with the concentration of Zn_2(DDSQ-ND). As can been seen, the endothermic peaks occurred at 118.3, 124.5, 125.6, 126.7, 127.1, 127.5, 127.7 and 127.8 °C for pure iPP with 0, 0.05, 0.1, 0.2, 0.4, 0.6, 0.8, and 1 wt % Zn_2(DDSQ-ND), respectively. The detailed data are summarized in Table 1. Compared with pure iPP, the results indicated that the T_c has been greatly improved for iPP/Zn_2(DDSQ-ND) composites. The decrease of supercooling (ΔT) of nucleated iPP, that is, the difference between T_c and T_m (the melting peak temperature), was also suggestive of a growing rate of crystallization, as proposed by Beck et al. [34]. As Table 1 shown, ΔT of pure iPP was 46.6 °C, while that of nucleated iPP was 35.8 °C (containing 1 wt % of Zn_2(DDSQ-ND)), lowered by 10.8 °C. The lower supercooling required for crystallization reflected that the crystallization could appear more easier and the crystallization rate is faster during practical application. Therefore, Zn_2(DDSQ-ND) accelerated the crystallization rate of iPP and acted as undoubtedly an effective nucleating agent in the system.

The melting curves of all the samples are shown in Fig. 4(b). The melting peak temperature (T_m) of the samples are listed in Table 1. It is observed that all the samples showed one endothermic peak, which belongs to the melting of α-formed crystal of iPP [35]. Combining the results of the cooling curve, it can be concluded that Zn_2(DDSQ-ND) acted as α-nucleating sites and significantly promoted the formation of α-phase iPP.

However, the cooling rate obtained by conventional DSC measurements could not match with the actual polymer processing [36]. DSC only achieves lower supercooling, which is often much lower than the actual cooling rate during processing. It is known from practice that high cooling rates of about 100–10000 °C s^{-1} occur during processing, such as blow molding and injection molding [36]. Ultra-fast scanning calorimetry (FSC) could provide convenient conditions for the study of the crystallization behaviors of polymer in much higher cooling rates than DSC. Herein, we choose the cooling rate of 200 °C s^{-1} to investigate the crystallization behaviors of all samples under a higher cooling rate (Fig. 6).

For the pure iPP, the FSC result showed two crystallization peaks in the cooling curves. The lower temperature peak occurred at around 15 °C, which is attributed to the formation of mesophase iPP due to the high cooling rate [37]. The higher crystallization temperature around 60 °C corresponds to the formation of stable α-phase iPP. The lower crystallization peak gradually disappeared with the content of Zn_2(DDSQ-ND) increasing in the system. When the content of Zn_2(DDSQ-ND) was higher than 0.2 wt %, there is no significant mesophase iPP generated, which denoted the heterogeneous nucleation effect of Zn_2(DDSQ-ND) in the iPP system. Besides, the higher crystallization peak temperature gradually increased as the content of Zn_2(DDSQ-ND) increased, as expected. The results are consistent with the conventional DSC.

During the heating process, the samples tended to reorganize and cold crystallization, which behaved as an exothermal peak of iPP at around 30 °C in Fig. 6(b). The mesophase melts around 80 °C and recrystallizes at about 100 °C [38]. Then, all formed crystals melt at a higher temperature of about 125 °C. With the addition of Zn_2(DDSQ-ND), the peak of the cold crystallization gradually disappeared and showed one exothermic peak. This phenomenon indicated that there has no obvious reorganization of the crystalline happened during heating and the formed crystal more stable for the iPP/Zn_2(DDSQ-ND) composites. Combined with the increased T_c, it can be concluded that Zn_2(DDSQ-ND) effectively suppressed the formation of mesophase iPP and the cold crystallization behavior and promoted

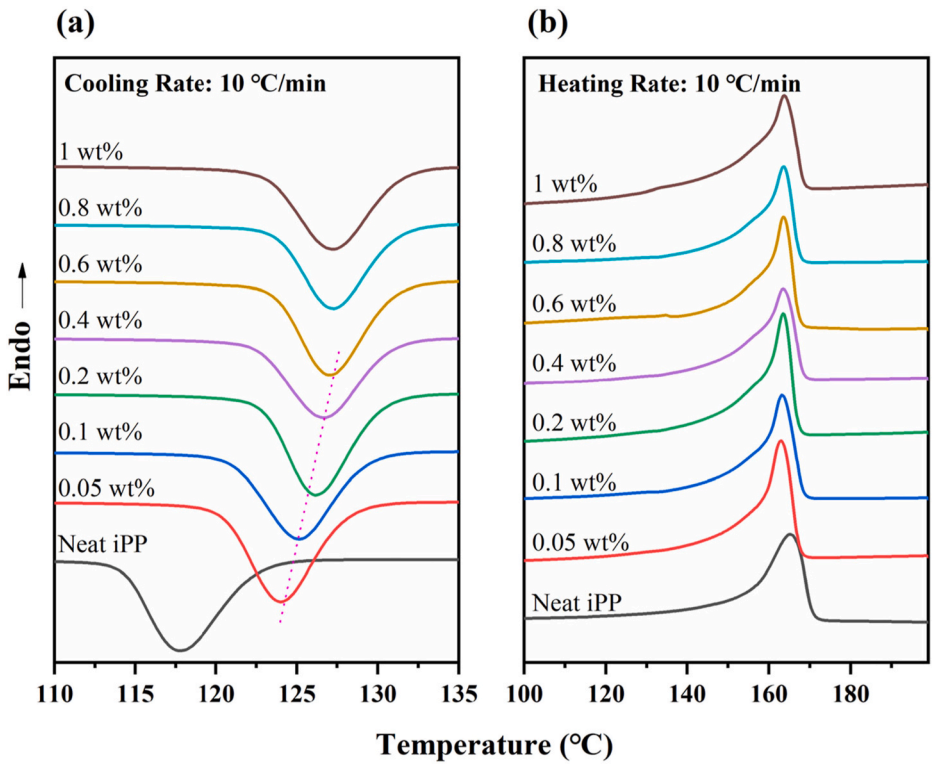

Fig. 4. The DSC curves of neat iPP and nucleated iPP with different content of Zn_2(DDSQ-ND) on the (a) first cooling and (b) second heating scan in N_2.

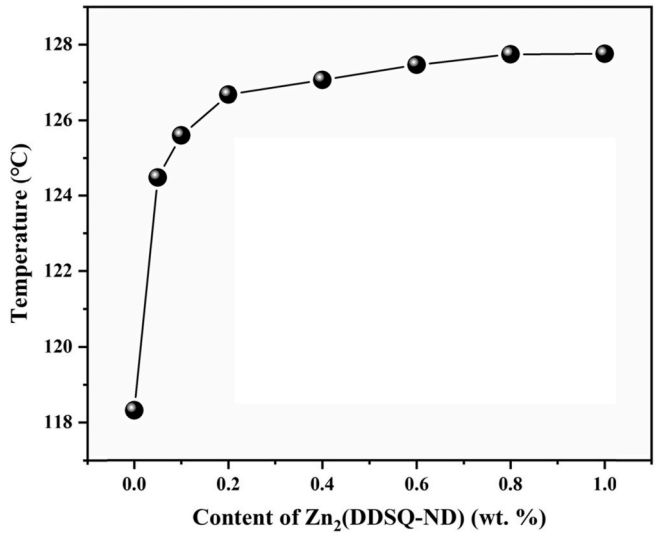

Fig. 5. The crystallization temperature of iPP with different content of Zn_2(DDSQ-ND).

the formation of α-phase iPP during the processing.

3.2. Crystal morphology

The morphologies of spherulites were investigated using polarized optical microscopy (POM). Fig. 7 presents the POM micrographs of neat iPP and iPP/Zn_2(DDSQ-ND) after completing the isothermal crystallization. For neat iPP, the crystals formed into larges spherulites due to their slow crystallization rate. With the addition of Zn_2(DDSQ-ND), the spherulite size significantly reduced and the nucleation densities dramatically increased. The reason for this phenomenon is the spherulites tended to impinge on other spherulites during the isothermal crystallization processing and stopped further growth, which resulted in smaller spherulites and increased spherulite number densities.

Table 1
Crystallization and melting behaviors of pure iPP and iPP/Zn_2(DDSQ-ND) composites obtained from DSC.

Samples	T_p (°C)	T_m (°C)	ΔT (°C)
Pure iPP	118.3	164.9	46.6
0.05 wt %	124.5	162.7	38.2
0.1 wt %	125.6	163.1	37.5
0.2 wt %	126.7	163.2	36.5
0.4 wt %	127.1	163.3	36.2
0.6 wt %	127.5	163.4	35.9
0.8 wt %	127.7	163.5	35.8
1 wt %	127.8	163.6	35.8

$\Delta T = T_m - T_c$.

The wide-angle X-ray diffraction (WAXD) patterns of pure iPP and nucleated iPP with different content of Zn_2(DDSQ-ND) are shown in Fig. 8. The WAXD results of iPP samples peak positions are consistent with that reported before [39], where its characteristic peaks can be found at 2θ angles of 14.14°(110), 16.96°(040), 18.56°(130), 21.25°(111) and 21.91°(131). It clearly indicated that all the iPP samples can only form α-crystal in the system. Therefore, the addition of Zn_2(DDSQ-ND) significantly reduced the sizes of iPP spherulites but did not change the crystal form of iPP. Besides, the characteristic peak of Zn_2(DDSQ-ND) was observed at 2θ angles of 6.59°. It can be clearly observed that the characteristic peak can be found when higher content of Zn_2(DDSQ-ND) is added in the iPP matrixes, which indicated that the Zn_2(DDSQ-ND) could crystallize in the iPP system. Similar results are also observed in other systems [40–42]. Combining the results of DSC, POM, and WAXD, it can be concluded here that Zn_2(DDSQ-ND) acted as an effective α-nucleating agent, which obviously enhanced the crystallization process and exhibited outstanding nucleation efficiency in the iPP system.

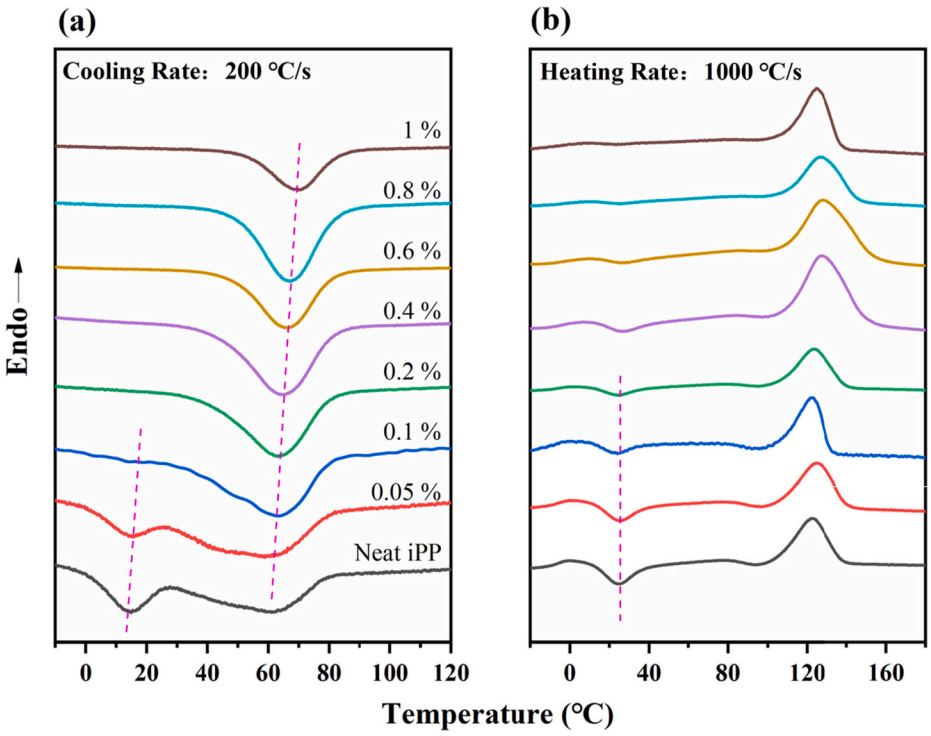

Fig. 6. The DSC (a) cooling and (b) heating curves of neat iPP and nucleated iPP with different content of Zn_2(DDSQ-ND) in N_2.

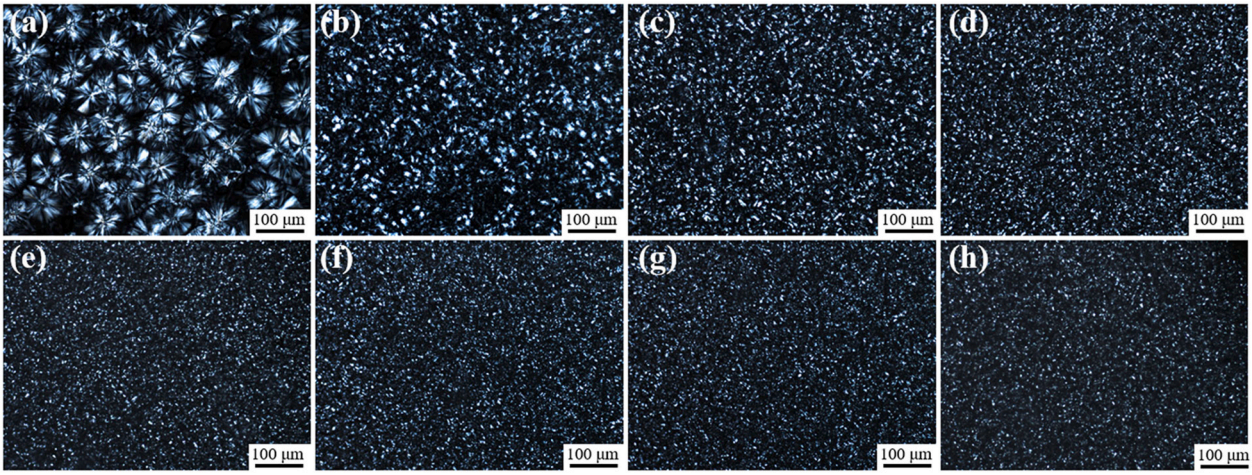

Fig. 7. Polarized optical microscope photographs of (a) pure iPP and nucleated iPP with (b) 0.05 wt %, (c) 0.1 wt %, (d) 0.2 wt %, (e) 0.4 wt %, (f) 0.6 wt %, (g) 0.8 wt % and (h) 1 wt % Zn_2(DDSQ-ND) after completing isothermal crystallization at 141 °C.

3.3. Non-isothermal crystallization behavior

The cooling rates have a dramatic impact on the crystallization behavior and the properties of the semi-crystalline polypropylene [43–49]. To further investigate the influence of the Zn_2(DDSQ-ND) on the crystallization behavior of iPP, the non-isothermal crystallization behaviors of the neat iPP and nucleated iPP with 0.2 wt % Zn_2(DDSQ-ND) were investigated using FSC under the cooling rate of 1–1000 °C s^{-1}.

As shown in Fig. 9, when the cooling rate was lower than 50 °C s^{-1}, the cooling process showed a single obvious exothermic event, which attributed to the crystallization of iPP. With the cooling rate increases, the T_c shifted toward the low temperature (as the orange line showed) and became broad because the crystals had less time to nucleate and grow [42]. The T_cs of the iPP/Zn_2(DDSQ-ND) composites were higher than that of the neat iPP. For the neat iPP, the exothermic peaks occurred at 105.1, 100.5, 95.4, 89.9, 84.6 and 77.1 °C at the cooling rate 1, 2, 5, 10, 20 and 50 °C s^{-1}, respectively; the T_cs of iPP/Zn_2(DDSQ-ND) were 109.8, 105.8, 100.6, 96.1, 90.7, 83.0 °C, respectively. At the same cooling rate, the T_c values of the iPP/Zn_2(DDSQ-ND) composite are always higher than that of pure iPP. The result had the same tendency as the traditional DSC results (Figs. 4–5).

When the cooling rate exceeded 50 °C s^{-1}, the cooling curve showed two exothermic peaks for the sample of pure iPP. A much lower crystallization peak was observed around 20 °C for the neat iPP, which was attributed to the mesophase formation. The phenomenon is related to the fact that α-crystallization is not completed at high temperatures due to rapid cooling rates, leaving enough supercooled melt for mesophase formation. However, there is no obvious mesophase formed in the iPP/Zn_2(DDSQ-ND) system when the cooling rate exceeded 50 °C s^{-1}, which

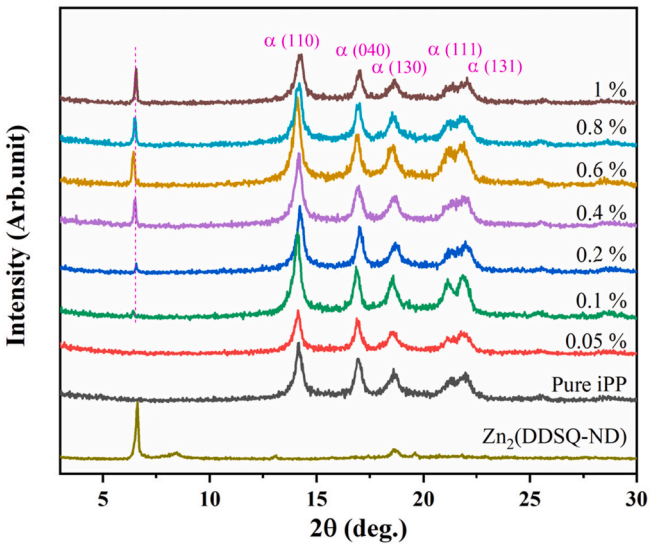

Fig. 8. WAXD profiles of pure Zn_2(DDSQ-ND), iPP and nucleated iPP samples with different content of Zn_2(DDSQ-ND).

indicated that Zn_2(DDSQ-ND) have a positive effect on the formation of more stable α-crystalline phase iPP under the high cooling rate and acted as a nucleating agent in the system. Besides, for all the samples, the intensity of the crystallization peak became weaker with higher cooling rates. When the cooling rate is too fast, there are no crystallization phenomenon was observed. This indicated that the crystallization behavior of iPP was suppressed and the material remains amorphous under fast cooling rates.

As is well-known, the melting behaviors of the polymers are closely related to their crystallization behaviors. Therefore, the corresponding melting behaviors of neat iPP and iPP/Zn_2(DDSQ-ND) were investigated using FSC. The heating rate used here is 1000 °C s^{-1}, which is well below the critical heating rate of iPP and allows for observing the cold crystallization behavior during heating [50]. Fig. 10 presents the FSC heating curves of the samples that crystallized at different cooling rates. It is clearly depicted that the glass transition happened as an endothermal peak at around 0 °C (see red symbols). Besides, the samples have cold crystallization, which happened at approximately 30 °C as the broad exothermal peak. The result is an indication that amorphous iPP is dominant in the sample, which is corresponding to the cooling curves. As the cooling rate gradually decreased, the intensity of the exothermic peak became weaker on the heating curve and the cold crystallization behavior gradually disappeared. This result is contributed to the crystals became more stable during the lower cooling rate. The critical cooling rate that formed cold crystallization is 50 °C s^{-1} for pure iPP and 100 °C s^{-1} for the iPP/Zn_2(DDSQ-ND), which suggested that the Zn_2(DDSQ-ND) improved the stability of the formed crystal. Besides, the small exothermic crystallization peaks around 100 °C are related to the recrystallization of the mesophase into α-phase [29]. All crystals melt at a higher temperature and shown one melting peak of approximately 120 °C, which belongs to the stable α-crystals of iPP.

When the cooling rates are further decreased (lower than 50 °C s^{-1} for pure iPP and 100 °C s^{-1} for iPP/Zn_2(DDSQ-ND)), the cold crystallization and reorganizations behavior (the mesophase to α-phase iPP) could not observe during the heating. The phenomenon attributed to that the stable α-phase crystals of iPP formed under a low cooling rate. Besides, the melting peak gradually shifted to a higher temperature with decreasing cooling rates, which related to the formed more perfect crystals under the lower cooling rates. Furthermore, the heat flow also clearly increased with the decrease of cooling rates because the melting enthalpy and crystallinity increased under a low cooling rate compared to a higher cooling rate.

As mentioned above, the evaluation of nucleation efficiency of the crystallization process is largely based on the T_c. Fig. 11 shows the T_cs of iPP with different content of Zn_2(DDSQ-ND) under different cooling rates. The T_c of samples was significant affected by the cooling rate. As the cooling rates increases, the T_c gradually shifted to a lower temperature. At the same cooling rate, the T_c of iPP/Zn_2(DDSQ-ND) is always higher than pure iPP, as shown in Fig. 11. Thus, the addition of

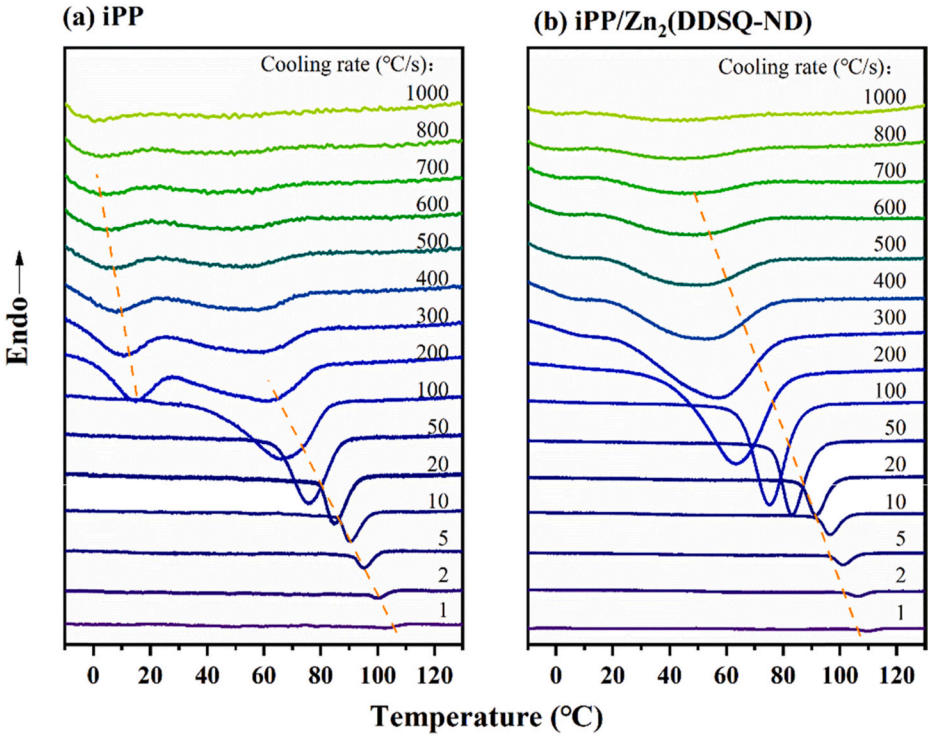

Fig. 9. The FSC curves of neat iPP and nucleated iPP with 0.02 wt % Zn_2(DDSQ-ND) at different cooling rates.

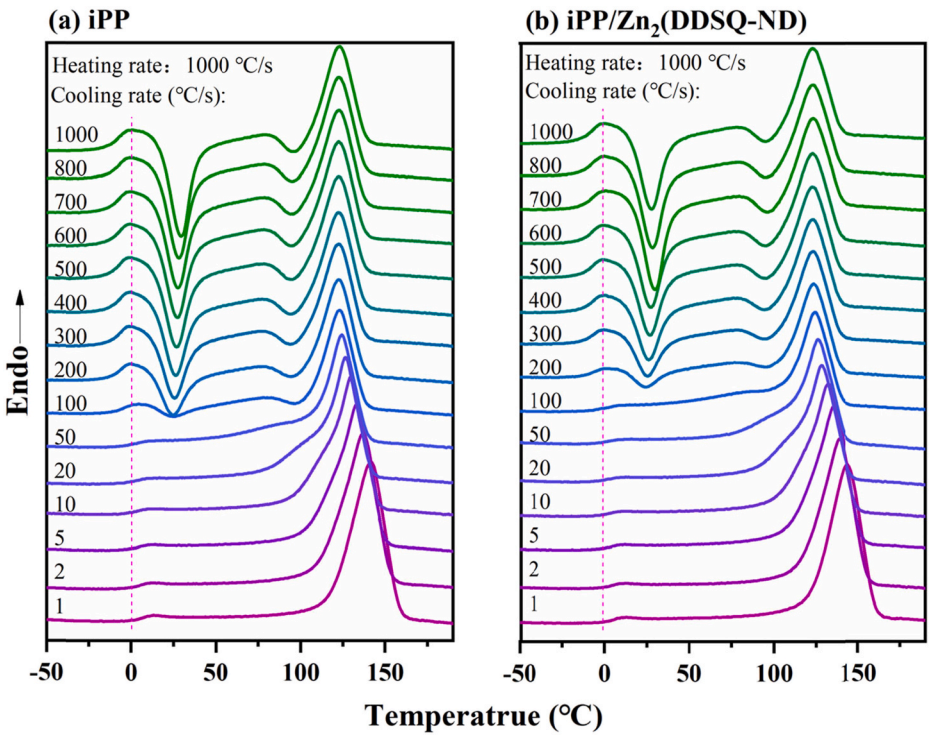

Fig. 10. The FDSC heating curves of (a) neat iPP and (b) Zn_2(DDSQ-ND)/iPP that crystallized under different cooling rates.

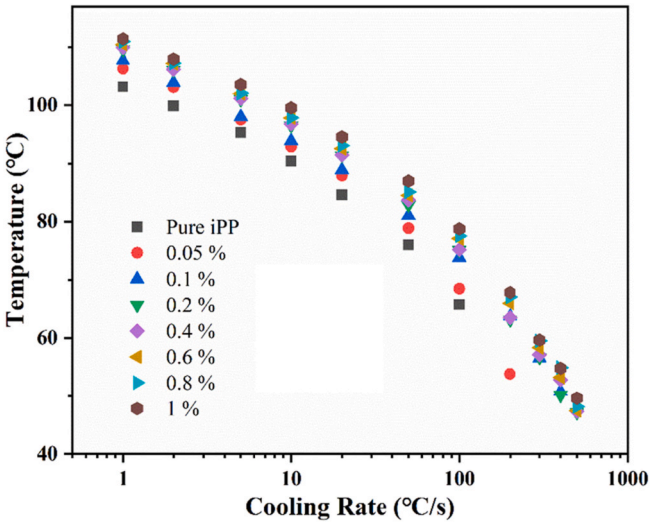

Fig. 11. Dependence of the crystallization peak temperatures on the cooling rates for the neat iPP and nucleated iPP with different content of Zn_2(DDSQ-ND).

Zn_2(DDSQ-ND) also accelerated the crystallization process under high cooling rates.

3.4. Isothermal crystallization behaviour

The heat flow rate of pure iPP and nucleated iPP with 0.2 wt % Zn_2(DDSQ-ND) was recorded in the isothermal crystallization process using FSC, as presented in Fig. 12. Under the different isothermal crystallization temperatures, it is evident that the trend of the maximum heat flow rate presented four regimes from the low to high crystallization temperature. Since the peak time of crystallization can determine by measuring the maximum heat flow rate of the samples during the isothermal processes, which is considered a convenient measure of the rate of phase transformation and a good approximation of half crystallization time [30,51]. As expected, the bimodal dependence of crystallization peak time as a function of the temperature was observed, as shown in Fig. 13. Two obvious minima of crystallization peak time for all the samples were observed at about 20 and 72 °C. It has been reported that the mesophase iPP was formed at the lower temperature and α-iPP formed at higher temperature [29]. Generally, at the higher supercooling, the samples have a higher thermodynamic driving force for crystallization and showed a lower peak time of crystallization. When the supercooling further increased, the mobility of the samples decreased and resulted in a lower crystallization rate and longer crystallization time [51]. Consequently, the minima of crystallization peak time of mesophase/α-phase iPP can be observed during the isothermal crystallization processing, and the respective nucleation schemes change at around 44 °C.

Notably, the crystallization rate of iPP is inversely proportional to the crystallization peak time. The results clearly showed that the addition of Zn_2(DDSQ-ND) reduced the isothermal crystallization peak time of α-phase iPP and significantly promoted its crystallization during the isothermal process. As shown in Fig. 14, the crystallization peak time decreases with increasing Zn_2(DDSQ-ND) content. Consequently, it acted as a heterogeneous nucleation site for iPP crystallization, which is in good agreement with the results of non-isothermal crystallization. Besides, the mesophase formation of iPP has not been significantly affected by the Zn_2(DDSQ-ND). The phenomenon is related to the existence of many mesophase nodules at low temperatures, the number of which exceeded conventional α-phase nucleating heterogeneities by several orders of magnitude [52]. Thus, the isothermal crystallization behavior of iPP has not been largely influenced by Zn_2(DDSQ-ND) in the mesophase formation area. Similar results have been found in other α-nucleating agents of iPP [29].

To get more information about the isothermal crystallization behavior, the heating curves also was measured using FSC after the isothermal crystallization of the samples was completed, as shown in Fig. 14. At the lower isothermal crystallization temperature, the melting

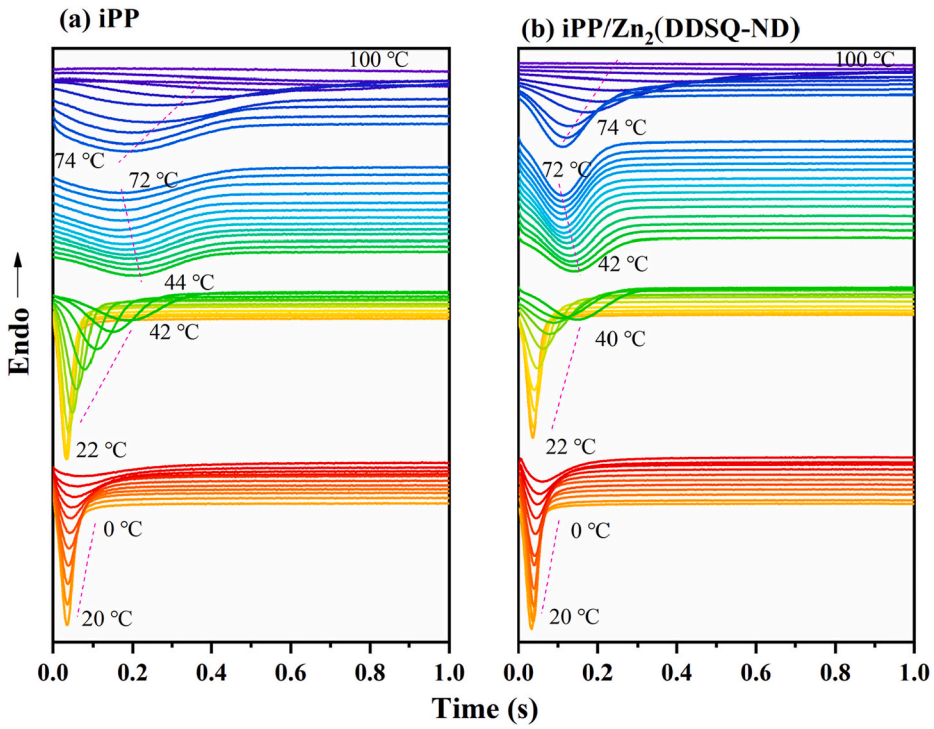

Fig. 12. FSC heat flow curves of (a) iPP and iPP with 0.2 wt% Zn_2(DDSQ-ND) at different isothermal temperature.

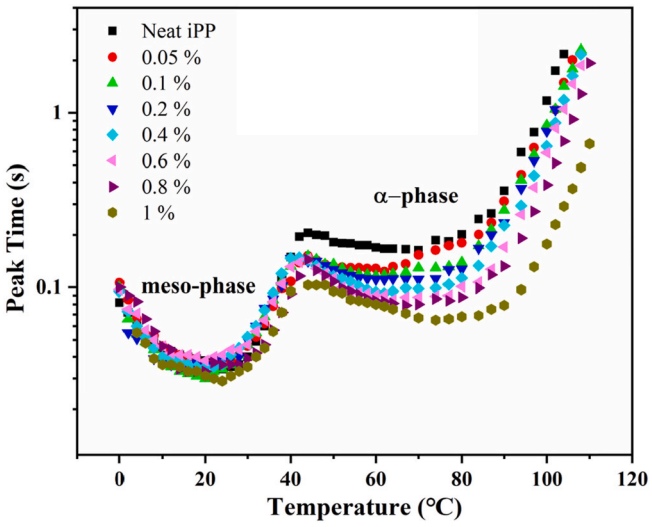

Fig. 13. Peak time of crystallization of pure iPP and iPP/Zn_2(DDSQ-ND) composites as a function of crystallization temperature.

of mesophase and the recrystallization (the mesophase into stable α-phase iPP) behavior was observed (see blue symbols), followed by the melting of the iPP crystals (see red symbols). Unlike non-isothermal crystallization, cold crystallization behavior was not observed in the heating curve after isothermal crystallization was completed. When the isothermal crystallization temperature was higher than 44 °C, the melting of mesophase and the recrystallization behavior could not be obviously observed, indicating crystals in the system are mainly the α-phase iPP. The results are consistent with the data discussed above. When the isothermal crystallization temperature further increased (74–97 °C), the melting peak gradually shifted to the higher temperature. Worth noting, the melting enthalpy for the pure iPP gradually decreased when the crystallization temperature further increased (higher 100 °C), while the samples iPP/Zn_2(DDSQ-ND) have no obvious change in melting enthalpy. The phenomenon suggested the Zn_2(DDSQ-ND) have a positive effect on isothermal crystallization under the higher temperature. Combining the improved crystallization temperature (isothermal and non-isothermal crystallization), Zn_2(DDSQ-ND) acted as an effectively α-nucleating agent in the iPP system.

4. Conclusion

The POSS-based nucleating agent Zn_2(DDSQ-ND) was firstly synthesized and the crystallization behaviors of the iPP/Zn_2(DDSQ-ND) composites were investigated using conventional DSC and FSC in detail. The results indicated that Zn_2(DDSQ-ND) acted as an effective nucleating agent in the iPP system. The crystallization peak temperatures greatly increased as the content of Zn_2(DDSQ-ND) increased. The nucleation density of iPP/Zn_2(DDSQ-ND) is higher than in pure iPP and the spherulites sizes of iPP are greatly reduced when Zn_2(DDSQ-ND) was added. The crystal structure of iPP remains unchanged in the composite based on the results of WAXD. Besides, due to the conventional DSC is not able to monitor the crystallization process under fast cooling and heating rates, the non-isothermal and isothermal crystallization behaviors of samples are characterized by the FSC. The results of non-isothermal crystallization under the cooling rates of 1–1000 °C s^{-1} revealed that Zn_2(DDSQ-ND) effectively suppressed the formation of mesophase iPP and the cold crystallization behavior and promoted the formation of α-phase iPP. The isothermal crystallization behaviors were further probed under a wider temperature range. The bimodal dependence of crystallization peak time as a function of the temperature was observed. Zn_2(DDSQ-ND) significantly improved the crystallization rate for the α-phase iPP when the isothermal crystallization temperature was above about 44 °C. Combining the results of non-isothermal and isothermal crystallization behavior, it can be concluded that the Zn_2(DDSQ-ND) acted as a novel and effective α-nucleation agent in the iPP system.

CRediT authorship contribution statement

Xian Zhang: Conceptualization, Methodology, Software, Validation,

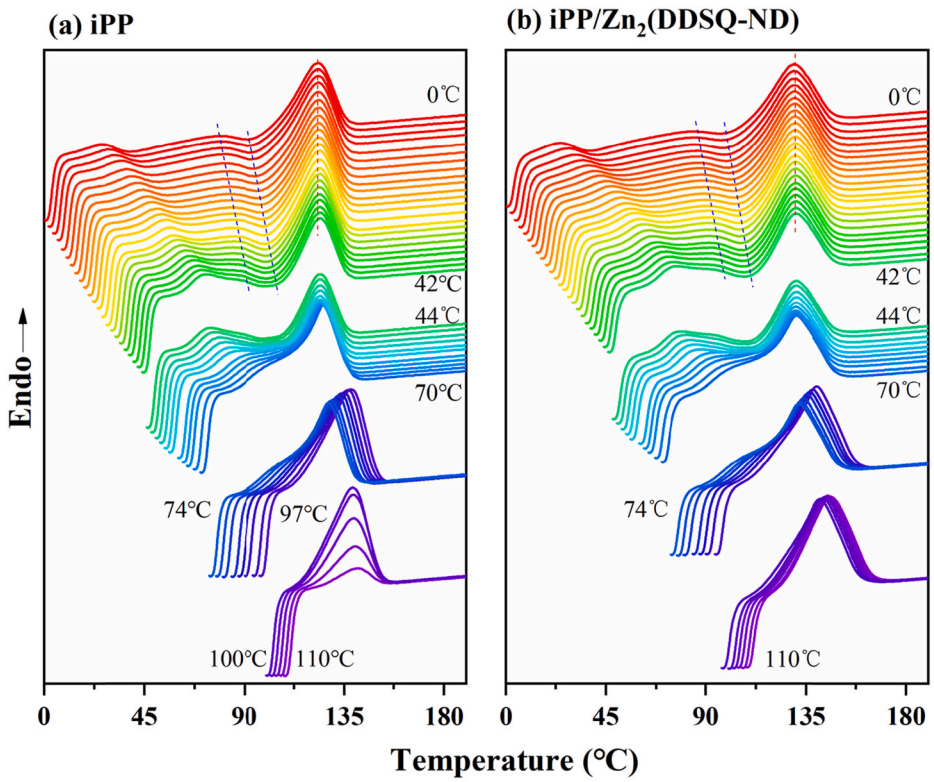

Fig. 14. FSC heating curves of (a) iPP and iPP with 0.2 wt% Zn_2(DDSQ-ND) after different isothermal temperature.

Formal analysis, Investigation, Data curation, Project administration, Writing – original draft, Visualization. **Shicheng Zhao:** Supervision, Resources, Project administration, Writing – review & editing, Funding acquisition. **Shiao-Wei Kuo:** Conceptualization, Resources, Writing-Reviewing. **Wei-Cheng Chen:** Resources, Writing-Reviewing. **Mohamed Gamal Mohamed:** Writing-Reviewing. **Zhong Xin:** Conceptualization, Supervision, Resources, Project administration, Writing – review & editing, Funding acquisition.

Declaration of competing interest

The authors declare that they have no known competing financial interests or personal relationships that could have appeared to influence the work reported in this paper.

Acknowledgements

This works was financially supported by National Natural Science Foundation of China (Grants 21878089 and 21606084), the National key R&D Program of China (2016YFB0302201) and the Fundamental Research Funds for the Central Universities (22221818010).

Appendix A. Supplementary data

Supplementary data to this article can be found online at https://doi.org/10.1016/j.polymer.2021.123574.

References

[1] C. Creton, Molecular stitches for enhanced recycling of packaging, Science 355 (2017) 797–798.
[2] C. De Rosa, F. Auriemma, Structural-mechanical phase diagram of isotactic polypropylene, J. Am. Chem. Soc. 128 (2006) 11024–11025.
[3] V. Busico, R. Cipullo, Microstructure of polypropylene, Prog. Polym. Sci. 26 (2001) 443–533.
[4] Y. Yang, Z. Xin, S. Zhao, Y. Shi, S. Zhou, J. Zhou, C. Ye, Nucleation effects of zinc adipate as β-Nucleating agent in ethylene-propylene block copolymerized polypropylene, J. Polym. Res. 24 (2017) 143.
[5] X. Peng, Z. Xin, S. Zhao, S. Zhou, Y. Shi, C. Ye, Unique crystallization behavior of isotactic polypropylene in the presence of l-isoleucine and its inhibition and promotion mechanism of nucleation, J. Appl. Polym. Sci. 135 (2018) 45956.
[6] C. De Rosa, F. Auriemma, O. Tarallo, A. Malafronte, R. Di Girolamo, S. Esposito, F. Piemontesi, D. Liguori, G. Morini, The "nodular" α form of isotactic polypropylene: stiff and strong polypropylene with high deformability, Macromolecules 50 (2017) 5434–5446.
[7] H. Niu, N. Wang, Y. Li, Influence of beta-nucleating agent dispersion on the crystallization behavior of isotactic polypropylene, Polymer 150 (2018) 371–379.
[8] X. Jiang, W. Zhang, S. Zhao, S. Zhou, Y. Shi, Z. Xin, Effect of benzoic acid surface modified alumina nanoparticles on the mechanical properties and crystallization behavior of isotactic polypropylene nanocomposites, RSC Adv. 8 (2018) 20790–20800.
[9] M. Guo, Y. Zhang, J. Li, G. Pan, H. Yan, Y. Luo, Y. Liu, Ultrafine dispersion of a phosphate nucleating agent in a polypropylene matrix via the microemulsion method, RSC Adv. 4 (2014) 11931.
[10] Y.F. Zhang, B. He, H. Hou, L. Guo, Isothermal crystallization of isotactic polypropylene nucleated with a novel aromatic heterocyclic phosphate nucleating agent, J. Macromol. Sci., Part B 56 (2017) 811–820.
[11] S. Teng, Z. Qiu, Nucleating and plasticization effects of low-loading octavinyl-polyhedral oligomeric silsesquioxanes in novel biodegradable poly(ethylene succinate-co-diethylene glycol succinate)-based nanocomposite, Ind. Eng. Chem. Res. 56 (2017) 14807–14813.
[12] M.G. Mohamed, S.W. Kuo, Functional polyimide/polyhedral oligomeric silsesquioxane nanocomposites, Polymers 11 (2019) 26.
[13] X. Zhang, S. Zhao, Z. Xin, The chain dis-entanglement effect of polyhedral oligomeric silsesquioxanes (POSS) on ultra-high molecular weight polyethylene (UHMWPE), Polymer 202 (2020) 122631.
[14] M.G. Mohamed, S.W. Kuo, Polybenzoxazine/Polyhedral oligomeric silsesquioxane (POSS) nanocomposites, Polymers 8 (2016) 225.
[15] A. Sellinger, R.M. Laine, Silsesquioxanes as synthetic platforms. Thermally curable and photocurable inorganic/organic hybrids, Macromolecules 29 (1996) 2327–2330.
[16] A. Romo Uribe, A. Reyes Mayer, M. Paredes Pérez, J. Lichtenhan, M. Yañez Lino, E. Sarmiento Bustos, POSS driven chain disentanglements, decreased the melt viscosity and reduced O2 transmission in polyethylene, Polymer 165 (2019) 61–71.
[17] W. Zhang, G. Caminob, R. Yang, Polymer/polyhedral oligomeric silsesquioxane (POSS) nanocomposites: an overview of fire retardance, Prog. Polym. Sci. 67 (2017) 77–125.
[18] S.W. Kuo, F.C. Chang, POSS related polymer nanocomposites, Prog. Polym. Sci. 36 (2011) 1649–1696.
[19] H. Sirin, D. Turan, G. Ozkoc, S. Gurdag, POSS reinforced PET based composite fibers: "Effect of POSS type and loading level", Compos. B Eng. 53 (2013) 395–403.

[20] S. Teng, Z. Qiu, Enhanced crystallization and mechanical properties of biodegradable poly(ethylene succinate) by octaisobutyl-polyhedral oligomeric silsesquioxanes in their nanocomposites, Thermochim. Acta 649 (2017) 22–30.
[21] M. Barczewski, M. Dobrzyńska-Mizera, M. Dutkiewicz, M. Szołyga, Novel polypropyleneβ-nucleating agent with polyhedral oligomeric silsesquioxane core: synthesis and application, Polym. Int. 65 (2016) 1080–1088.
[22] E.L. Heeley, D.J. Hughes, Y. El Aziz, P.G. Taylor, A.R. Bassindale, Morphology and crystallization kinetics of polyethylene/long alkyl-chain substituted Polyhedral Oligomeric Silsesquioxanes (POSS) nanocomposite blends: a SAXS/WAXS study, Eur. Polym. J. 51 (2014) 45–56.
[23] F. Carniato, A. Fina, D. Tabuani, E. Boccaleri, Polypropylene containing Ti- and Al-polyhedral oligomeric silsesquioxanes: crystallization process and thermal properties, Nanotechnology 19 (2008) 475701.
[24] F.X. Perrin, D.M. Panaitescu, A.N. Frone, C. Radovici, C. Nicolae, The influence of alkyl substituents of POSS in polyethylene nanocomposites, Polymer 54 (2013) 2347–2354.
[25] W. Qin, Z. Xin, C. Pan, S. Sun, X. Jiang, S. Zhao, In situ formation of zinc phthalate as a highly dispersed β-nucleating agent for mechanically strengthened isotactic polypropylene, Chem. Eng. J. 358 (2018) 1243–1252.
[26] S. Zhao, H. Gong, X. Yu, Z. Xin, S. Sun, S. Zhou, Y. Shi, A highly active and selective β-nucleating agent for isotactic polypropylene and crystallization behavior of β-nucleated isotactic polypropylene under rapid cooling, J. Appl. Polym. Sci. 133 (2016).
[27] Z. Lv, Y. Yang, R. Wu, Y. Tong, Design and properties of a novel nucleating agent for isotactic polypropylene, Mater. Des. 37 (2012) 73–78.
[28] Y. Zhang, X. Lin, S. Chen, Preparation and nucleation effect of a novel compound nucleating agent carboxylated graphene/calcium pimelate for isotactic polypropylene, J. Therm. Anal. Calorim. 136 (2019) 2363–2371.
[29] J.E.K. Schawe, P. Pötschke, I. Alig, Nucleation efficiency of fillers in polymer crystallization studied by fast scanning calorimetry: carbon nanotubes in polypropylene, Polymer 116 (2017) 160–172.
[30] J.E.K. Schawe, F. Budde, I. Alig, Nucleation activity at high supercooling: sorbitol-type nucleating agents in polypropylene, Polymer 153 (2018) 587–596.
[31] W.C. Chen, S.W. Kuo, Ortho-imide and allyl groups effect on highly thermally stable polybenzoxazine/double-decker-shaped polyhedral silsesquioxane hybrids, Macromolecules 51 (2018) 9602–9612.
[32] J.E.K. Schawe, Identification of three groups of polymers regarding their non-isothermal crystallization kinetics, Polymer 167 (2019) 167–175.
[33] F. Rybnikář, Efficiency of nucleating additives in polypropylene, J. Appl. Polym. Sci. 13 (1969) 827–833.
[34] H.N. Beck, H.D.J. Ledbetter, DTA study of heterogeneous nucleation of crystallization in polypropylene, J. Appl. Polym. Sci. 9 (6) (1965) 2131–2142.
[35] Y.F. Zhang, Crystallization and melting behaviors of isotactic polypropylene nucleated with compound nucleating agents, J. Polym. Sci., Part B: Polym. Phys. 46 (2008) 911–916.
[36] C. Schick, V. Mathot, Fast Scanning Calorimetry, Springer, 2016.
[37] J.E.K. Schawe, F. Budde, I. Alig, Non-isothermal crystallization of polypropylene with sorbitol-type nucleating agents at cooling rates used in processing, Polym. Int. 68 (2019) 240–247.
[38] R. Androsch, M.L. Di Lorenzo, C. Schick, B. Wunderlich, Mesophases in polyethylene, polypropylene, and poly(1-butene), Polymer 51 (2010) 4639–4662.
[39] R. Yang, L. Ding, W. Chen, L. Chen, X. Zhang, J. Li, Chain folding in main-chain liquid crystalline polyester with strong π–π interaction: an efficient β-nucleating agent for isotactic polypropylene, Macromolecules 50 (2017) 1610–1617.
[40] J.H. Chen, B.X. Yao, W.B. Su, Y.B. Yang, Isothermal crystallization behavior of isotactic polypropylene blended with small loading of polyhedral oligomeric silsesquioxane, Polymer 48 (2007) 1756–1769.
[41] J.H. Chen, Y.D. Chiou, Crystallization behavior and morphological development of isotactic polypropylene blended with nanostructured polyhedral oligomeric silsesquioxane molecules, J. Polym. Sci., Part B: Polym. Phys. 44 (2006) 2122–2134.
[42] X. Zhang, S. Zhao, M.G. Mohamed, S. Kuo, Z. Xin, Crystallization behaviors of poly (ethylene terephthalate) (PET) with monosilane isobutyl-polyhedral oligomeric silsesquioxanes (POSS), J. Mater. Sci. 55 (2020) 14642–14655.
[43] F. De Santis, S. Adamovsky, G. Titomanlio, C. Schick, Scanning nanocalorimetry at high cooling rate of isotactic polypropylene, Macromolecules 39 (2006) 2562–2567.
[44] F. De Santis, S. Adamovsky, G. Titomanlio, C. Schick, Isothermal nanocalorimetry of isotactic polypropylene, Macromolecules 40 (2007) 9026–9031.
[45] N. Mahmood, I. Kolesov, R. Glüge, H. Altenbach, R. Androsch, M. Beiner, Influence of structure gradients in injection moldings of isotactic polypropylene on their mechanical properties, Polymer 200 (2020) 122556.
[46] M. Gahleitner, D. Mileva, D. Gloger, R. Androsch, D. Tranchida, Polymer structure effects on crystallization and properties in polypropylene film casting, AIP Conference Proceedings 1914 (2017) 130001.
[47] S.A.E. Boyer, J.M. Haudin, Crystallization of polymers at constant and high cooling rates: a new hot-stage microscopy set-up, Polym. Test. 29 (2010) 445–452.
[48] K. Nishida, K. Okada, H. Asakawa, G. Matsuba, K. Ito, T. Kanaya, K. Kaji, In situ observations of the mesophase formation of isotactic polypropylene—a fast time-resolved X-ray diffraction study, Polym. J. 44 (2012) 95–101.
[49] D. Mileva, R. Androsch, D. Cavallo, G.C. Alfonso, Structure formation of random isotactic copolymers of propylene and 1-hexene or 1-octene at rapid cooling, Eur. Polym. J. 48 (2012) 1082–1092.
[50] J.E.K. Schawe, Analysis of non-isothermal crystallization during cooling and reorganization during heating of isotactic polypropylene by fast scanning DSC, Thermochim. Acta 603 (2015) 85–93.
[51] F. Paolucci, D. Baeten, P.C. Roozemond, B. Goderis, G.W.M. Peters, Quantification of isothermal crystallization of polyamide 12: modelling of crystallization kinetics and phase composition, Polymer 155 (2018) 187–198.
[52] L. Wang, K. Okada, M. Sodenaga, Y. Hikima, M. Ohshima, T. Sekiguchi, H. Yano, Effect of surface modification on the dispersion, rheological behavior, crystallization kinetics, and foaming ability of polypropylene/cellulose nanofiber nanocomposites, Compos. Sci. Technol. 168 (2018) 412–419.